

Fig. S1 Cross section of the NMC cathode acquired by FIB-SEM showing the random crystallographic orientations of the primary particles.

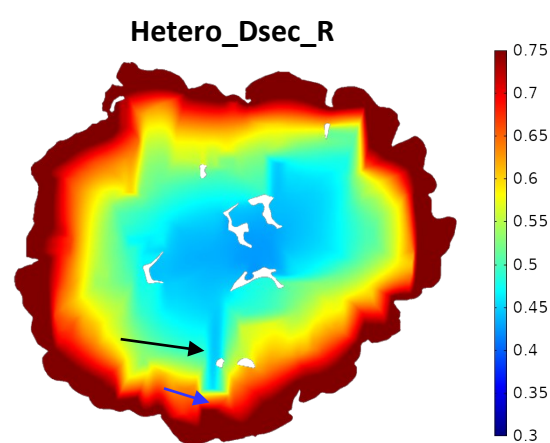


Fig. S2 SoL map of the NMC622 particle from Fig. 1 simulated using a reversed orientation vs. brightness relationship.

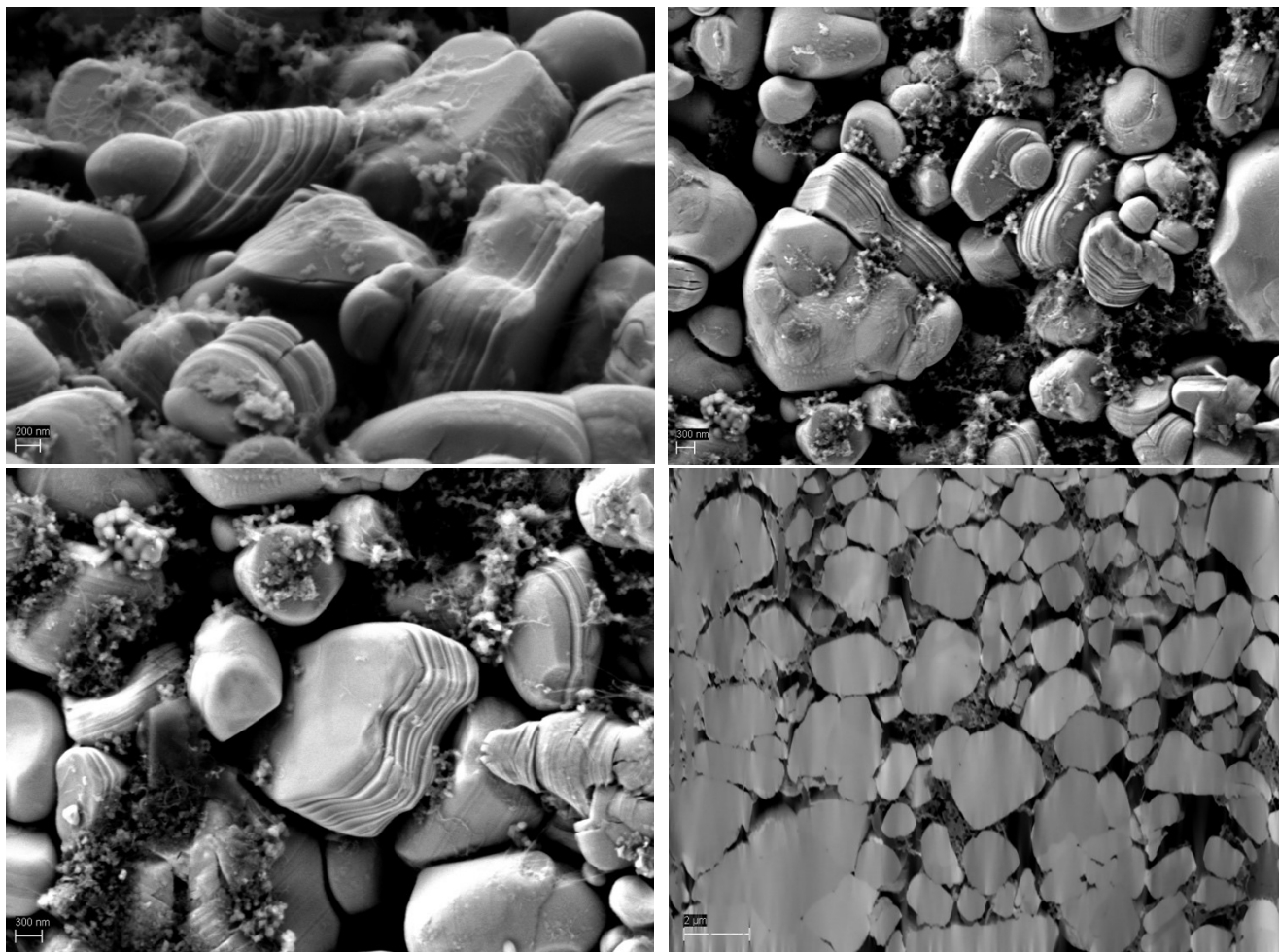


Fig. S3 SEM images of the SC NMC electrode. Planar features are informative of the crystal orientation.

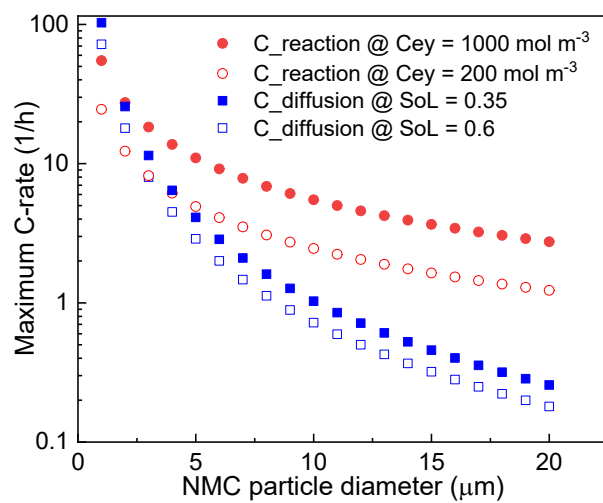


Fig. S4 Maximum C-rate limited by reaction kinetics and solid-state diffusion at different electrolyte concentration and SoL respectively.

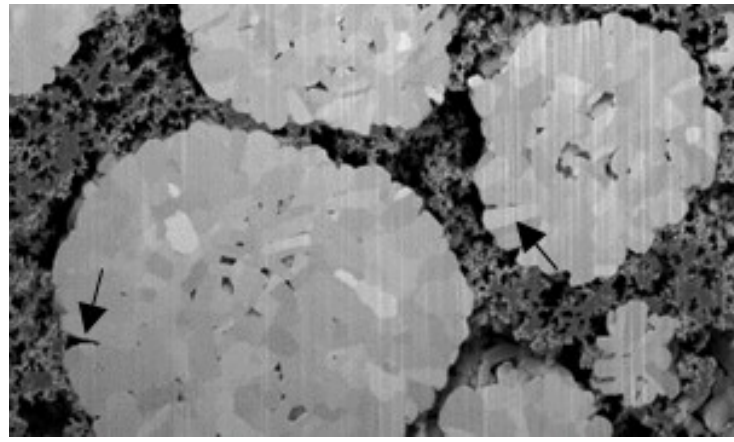


Fig. S5 SEM image showing surface cracks at the outer surface of NMC622 particles (indicated by black arrows).

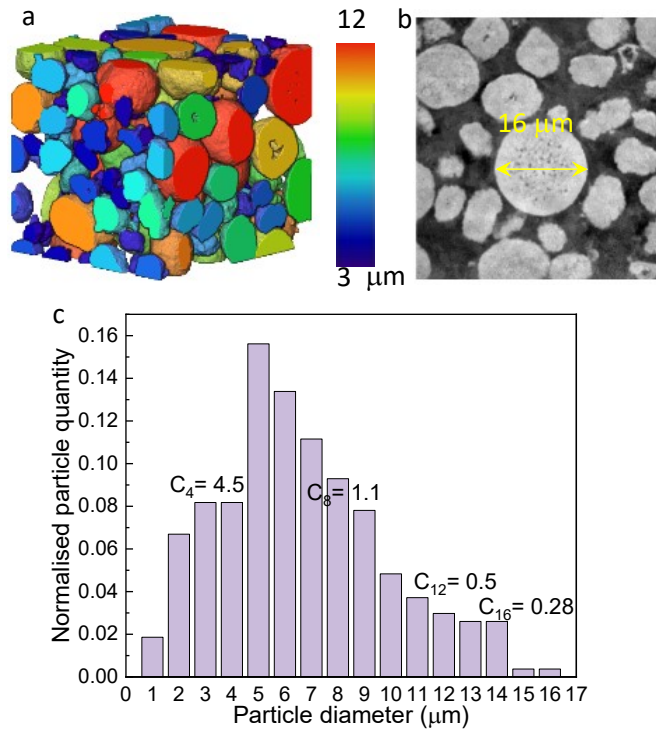


Fig. S6 (a) 3D visualization of the PSD in a commercial NMC622 electrode; (b) a cross-sectional view of the corresponding electrode obtained by X-ray nano-CT; (c) quantification of the PSD, shown alongside the maximum C-rate calculated based on the diffusion time constant t_d ($t_d = r^2/D_s$, r is the particle radius) and is calculated as $C_t = 3600/t_d$.

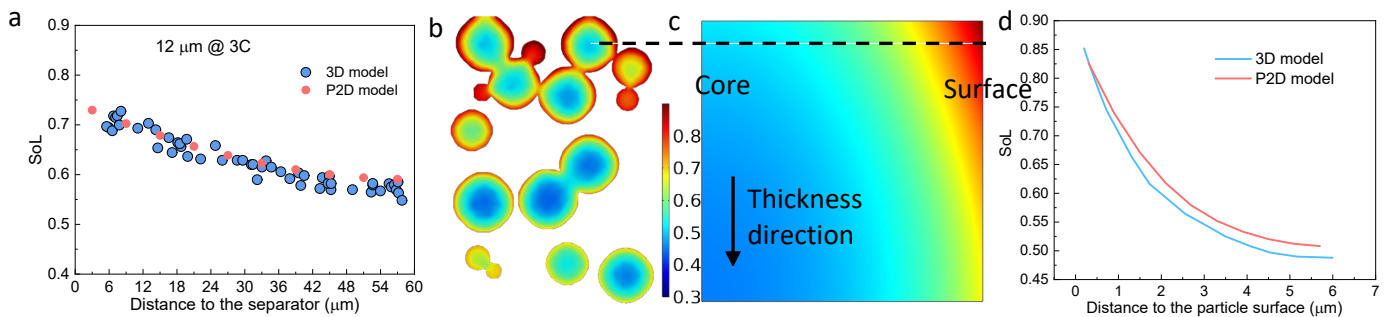


Fig. S7 Comparison of the results obtained by 3D and P2D modelling methods for ϵ_{H} electrode. (a) SoL distribution for the two methods across the thickness direction; (b) a slice of the SoL map of the particles obtained by 3D modelling; (c) SoL map obtained by P2D modelling (vertical axis is the thickness direction, horizontal axis is the radial particle direction). The core and outer surface of the particle are marked. The line profile of the SoL in a single particle is compared in (d).

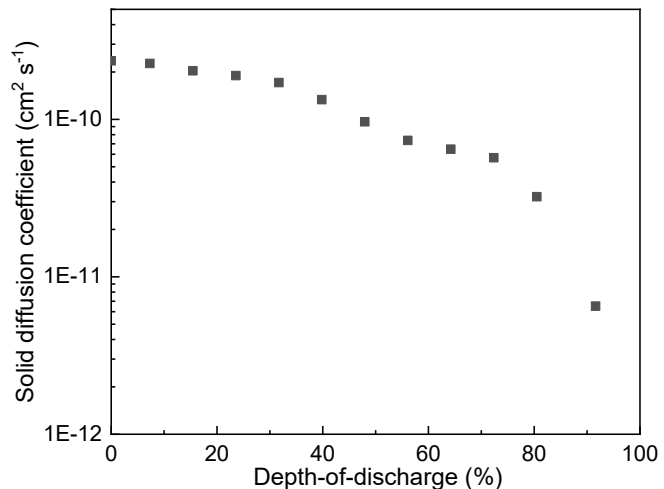


Fig. S8 Solid state diffusion coefficients of NMC622 as a function of the lithiation level using GITT technique¹.

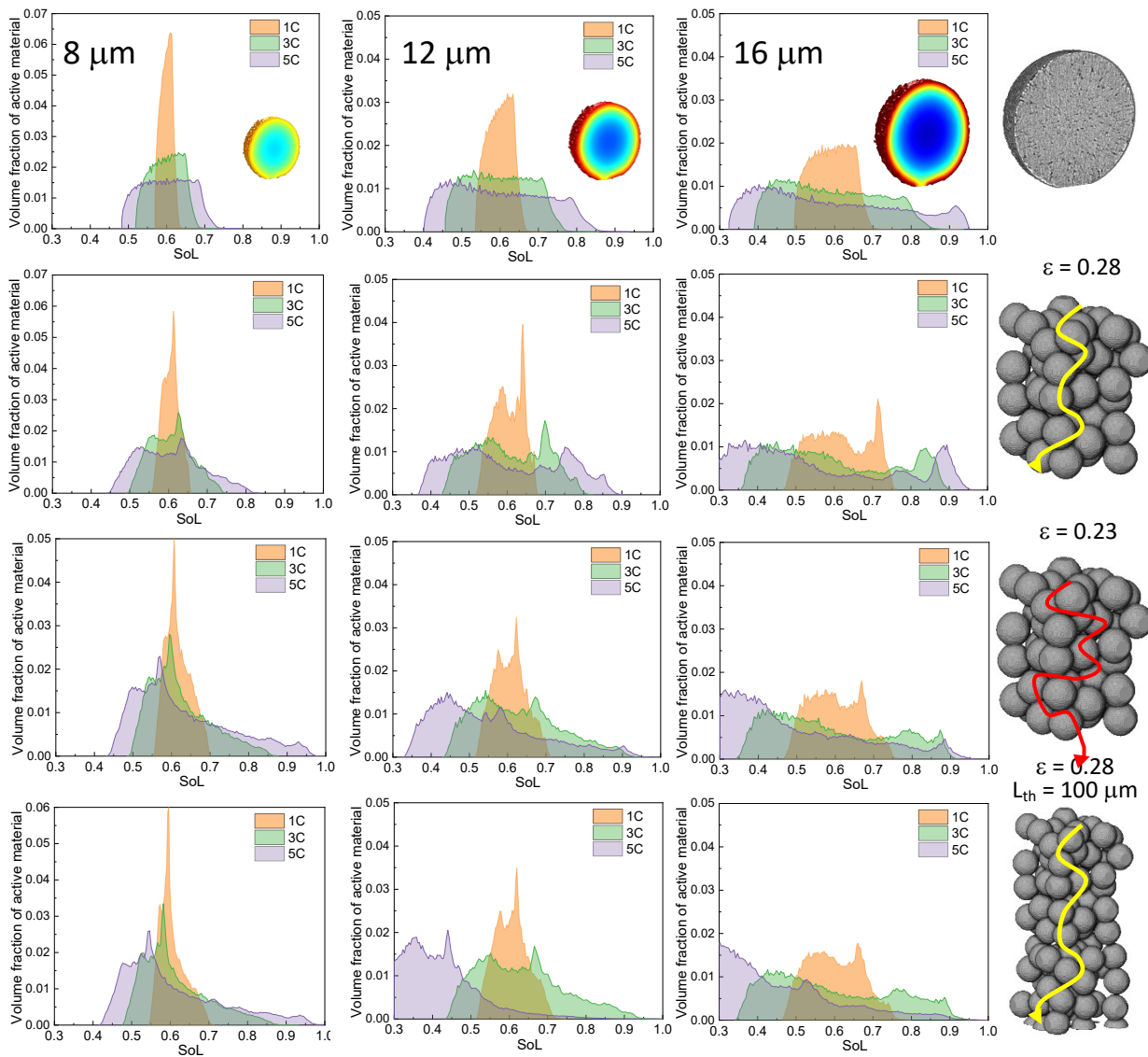


Fig. S9 SoL distribution shown as histogram for different electrodes with varying particle size.

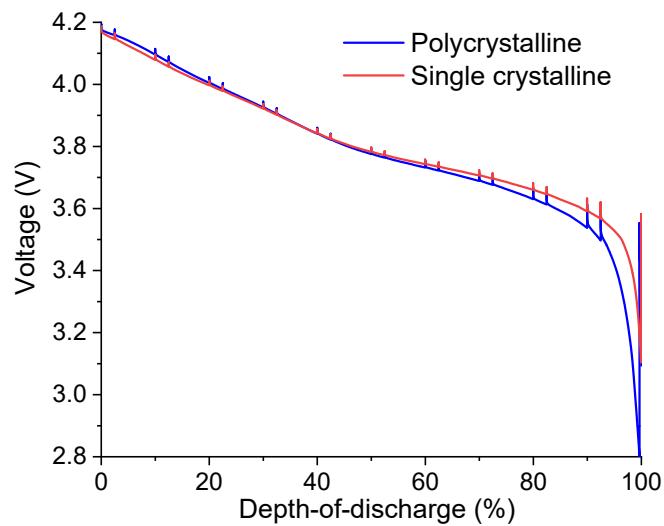


Fig. S10 GITT measurement on single and polycrystalline NMC811 electrode using coin cell (half cell, vs. lithium).

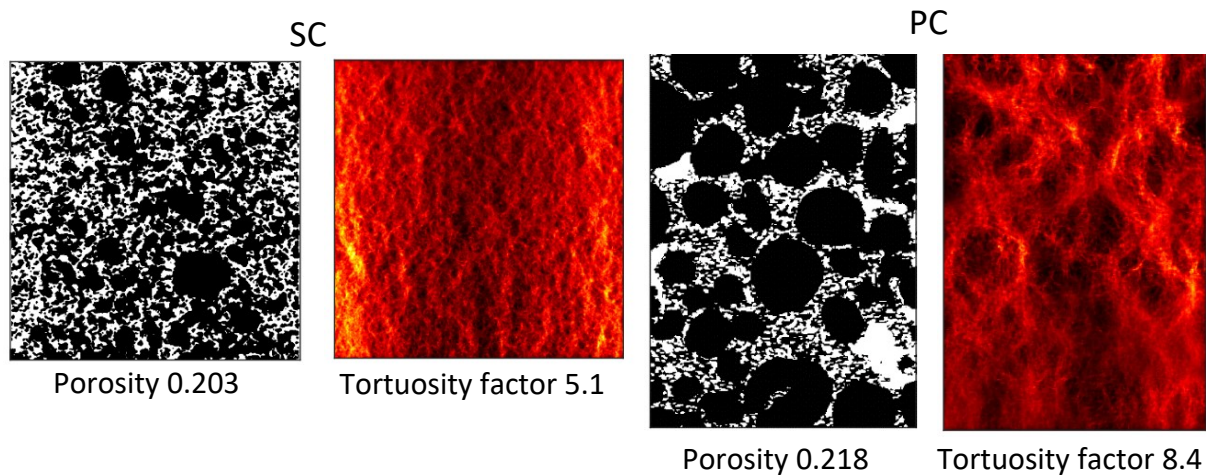


Fig. S11 Porosity (left, white phase) and tortuosity factor for the SC and PC electrodes. The former is obtained by image analysis and the latter is obtained by CFD simulation. Flux maps are shown here in terms of the 2D projection of all the slices.

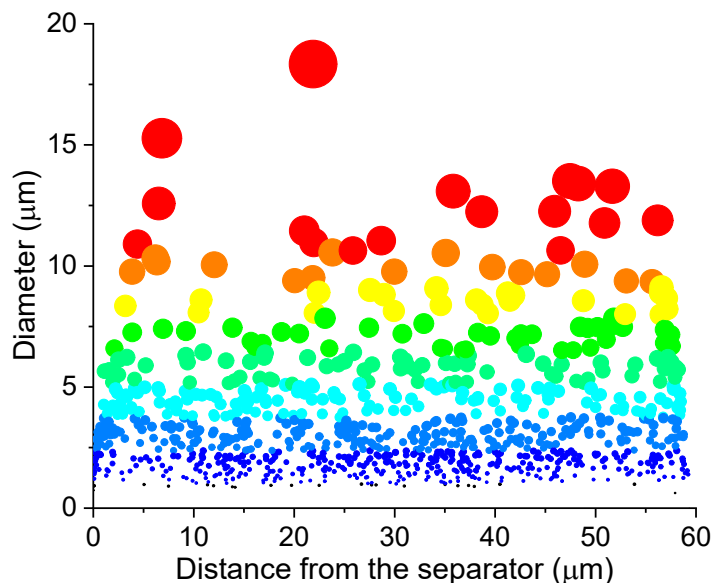


Fig. S12 PSD as a function of the distance from the separator in the PC electrode. The colormap corresponds to the particle size shown as the y-axis.

2D and 3D microstructure-resolved battery model

Nomenclature

variable/parameters

OCV	open circuit voltage, V
J_p	current density associated with flux of positive ion (Li^+), A m^{-2}
J_n	current density associated with flux of negative ion (X^-), A m^{-2}
J_e	current density associated with flux of electrons (e^-), A m^{-2}
J_s	flux of lithium ion intercalated in the active material, A m^{-2}
μ_p	potential in ion conducting phase, V
μ_e	potential in electron conducting phase, V
C_{ey}	concentration of the electrolyte salt, mol m^{-3}

C_{in}	initial electrolyte concentration, mol m ⁻³
c_s	lithium concentration in the active material, mol m ⁻³
$cmax_s$	maximum lithium concentration in the active material, mol m ⁻³
cin_s	initial lithium concentration in the active material, mol m ⁻³
$cacc_s$	accessible lithium concentration in the active material, mol m ⁻³
SoL_{in}	initial state of lithiation in the active material
SoL_{acc}	accessible state of lithiation in the active material
t_p	transference number of positive ion
σ_{io}	ionic conductivity in the electrolyte, S m ⁻¹
D_{io}	ambipolar diffusion coefficient of the binary electrolyte, m ² s ⁻¹
σ_e	electronic conductivity of the solid material, S m ⁻¹
D_s	solid state diffusion coefficient in active material, m ² s ⁻¹
i_{00}	reaction rate constant, A m ^{2.5} mol ^{-1.5}
i_0	exchange current density, A m ⁻²
J_{ct}	charge transfer current density, A m ⁻²
α	Transfer coefficient for intercalation half-reaction
I	applied current, A
A_e	area of the electron conducting materials on the inlet surface
V_{AM}	volume fraction of the active material in the electrode
V_{Pore}	porosity in the lumped CBD+pore phase ($= \varepsilon_{\text{electrode}} / (1 - V_{AM})$)
V_{CBD}	Volume fraction of the CBD in the lumped CBD+pore phase ($= 1 - V_{Pore}$)
τ_{CBD}	Tortuosity of the CBD in the lumped CBD+pore phase
τ_{Pore}	Tortuosity of the pore in the lumped CBD+pore phase
V	total volume of the electrode, m ³
A	cross sectional area of the inlet surface, m ²
F	Faraday constant, C mol ⁻¹
T	temperature, K
R	gas constant, J mol ⁻¹ K ⁻¹
V_{eq}	equilibrium potential at the active material/electrolyte interface, V

Table S1. Balance equations and flux equations

Domain: Pore + CBD (hybrid)	
Balance equation	Flux equation
$V_{pore}F \frac{\partial C_{ey}}{\partial t} + \nabla \cdot J_p = 0 \quad \text{* MERGEFORMAT (10)}$	$J_p = -t_p \frac{V_{pore}}{\tau_{pore}} \sigma_{io} \nabla \mu_p \quad \text{* MERGEFORMAT (13)}$
$-V_{pore}F \frac{\partial C_{ey}}{\partial t} + \nabla \cdot J_n = 0 \quad \text{* MERGEFORMAT (11)}$	$J_n = \frac{1}{t_p} F \frac{V_{pore}}{\tau_{pore}} D_{io} \nabla C_{ey} - (1-t_p) \frac{V_{pore}}{\tau_{pore}} \sigma_{io} \nabla \mu_p \quad \text{* MERGEFORMAT (14)}$
$\nabla \cdot J_e = 0 \quad \text{* MERGEFORMAT (12)}$	$J_e = -\frac{V_{CBD}}{\tau_{CBD}} \sigma_e \nabla \mu_e \quad \text{* MERGEFORMAT (15)}$
Domain: NMC particles	
$F \frac{\partial c_s}{\partial t} + \nabla \cdot J_s = 0 \quad \text{* MERGEFORMAT (16)}$	$J_s = -FD_s \nabla c_s \quad \text{* MERGEFORMAT (18)}$
$\nabla \cdot J_e = 0 \quad \text{* MERGEFORMAT (17)}$	$J_e = -\sigma_e \nabla \mu_e \quad \text{* MERGEFORMAT (19)}$
NMC/Pore interface	
Charge transfer kinetics	
$J_{ct} = i_0 \left[\exp\left(\frac{\alpha F}{RT} (\mu_p - \mu_e + V_{eq})\right) - \exp\left(-\frac{(1-\alpha)F}{RT} (\mu_p - \mu_e + V_{eq})\right) \right] \quad \text{* MERGEFORMAT (8)}$	$i_0 = i_{00} C_{ey}^\alpha c_s^\alpha (c_s^{\max} - c_s)^{1-\alpha} \quad \text{* MERGEFORMAT (9)}$

Table S2. Boundary conditions

Boundary: Separator/Electrode	$\mu_p = 0, n \cdot J_n = 0, n \cdot J_s = 0, n \cdot J_e = 0$
Boundary: Pore/NMC	$n \cdot J_p = J_{ct}, n \cdot J_n = 0, n \cdot J_s = J_{ct}, n \cdot J_e = J_{ct}$
Boundary: Electrode/Current collector	$n \cdot J_p = 0, n \cdot J_n = 0, n \cdot J_s = 0, n \cdot J_e = \frac{I}{A_e},$ $I = (c_s^{acc} - c_s^{in})V_{AM}V \frac{F}{3600} \frac{C_{rate}}{A}, c_s^{acc} = c_s^{\max} \times SoL_{acc}, c_s^{in} = c_s^{\max} \times SoL_{in}$

Initial Conditions:

$$C_{ey} = C_{in}, \mu_p = 0, c_s = c_s^{in}, \mu_e = OCV$$

Table S3. Input parameters for different simulations

<i>Parameters and domains</i>		
NMC	NMC622	NMC811
$D_s/m^2 s^{-1}$	From Fig. 6S ¹	From Fig. 7h
$\sigma_e/S m^{-1}$		1.039×10^{-3} ²
$c_{\max} s/mol m^{-3}$	32000	43623 (AC) 40841 (PC)
SoL_{in}	0.2	0.3
SoL_{\max}	1	1
OCV	Previous measurement ¹	From Fig. 7g
V_{AM}	0.43	0.605 (SC) 0.621 (PC)
Electrolyte		
$D_{io}/m^2 s^{-1}$	$10^{-4} \times 10^{-4.43-(54/(T-229-5.0 \times 10^{-3} C_{ey}))} - 0.22 \times 10^{-3} C_{ey}$ ³	
	$\sigma_{io} = 10^{-4} \times C_{ey} (-10.5 + 0.668 \times 10^{-3} C_{ey} + 0.494 \times 10^{-6} C_{ey}^{-2}$ $+ 0.074 T - 1.78 \times 10^{-5} C_{ey} T - 8.86 \times 10^{-10} C_{ey}^{-2} T$ $- 6.96 \times 10^{-5} T^2 + 2.8 \times 10^{-8} C_{ey} T^2)^2$ ³	
$C_{in}/mol m^{-3}$	800	
t_p	0.38	
V_{Pore} ($= \varepsilon_{electrode} / (1 - V_{AM})$)	0.5 (ε_H) 0.4 (ε_L)	0.51 (SC) 0.57 (PC)
τ_{Pore}	4 ¹ (ε_H) 8 ¹ (ε_L)	5.1 (SC) 8.4 (PC)
CBD		
$\sigma_e/S m^{-1}$		0.375×10^3 ⁴
V_{CBD} ($= 1 - V_{Pore}$)	0.5 (ε_H) 0.6 (ε_L)	0.49 (SC) 0.43 (PC)
τ_{CBD}	4 (ε_H) 8 (ε_L)	5.1 (SC) 8.4 (PC)
Reaction kinetics		
$i_{00}/A m^{2.5} mol^{1.5}$		5×10^{-7} ⁵
α	0.5	
$F/C mol^{-1}$	96485	
$R/J mol^{-1} K^{-1}$	8.314	
T/K	298	

References

1. Lu, X., Daemi, S.R., Bertei, A., Kok, M.D., O'Regan, K.B., Rasha, L., Park, J., Hinds, G., Kendrick, E., and Brett, D.J.J.J. (2020). Microstructural Evolution of Battery Electrodes During Calendering.
2. Park, M., Zhang, X., Chung, M., Less, G.B., and Sastry, A.M. (2010). A review of conduction phenomena in Li-ion batteries. *J. Power Sources* 195, 7904-7929.

3. Cai, L., and White, R.E. (2011). Mathematical modeling of a lithium ion battery with thermal effects in COMSOL Inc. Multiphysics (MP) software. *J. Power Sources* **196**, 5985-5989.
4. Liu, G., Zheng, H., Kim, S., Deng, Y., Minor, A.M., Song, X., and Battaglia, V.S. (2008). Effects of Various Conductive Additive and Polymeric Binder Contents on the Performance of a Lithium-Ion Composite Cathode. *J. Electrochem. Soc.* **155**, A887-A892.
5. Tsai, P.-C., Wen, B., Wolfman, M., Choe, M.-J., Pan, M.S., Su, L., Thornton, K., Cabana, J., Chiang, Y.-M.J.E., and Science, E. (2018). Single-particle measurements of electrochemical kinetics in NMC and NCA cathodes for Li-ion batteries. *11*, 860-871.